

# Optimal linear growth in swept boundary layers

By PETER CORBETT<sup>1</sup>† AND ALESSANDRO BOTTARO<sup>2</sup>

<sup>1</sup>Laboratoire de Mécanique des Fluides, École Polytechnique Fédérale de Lausanne,  
CH-1015 Lausanne, Switzerland

<sup>2</sup>Institut de Mécanique des Fluides de Toulouse, Allée du Pr. Camille Soula,  
F-31400 Toulouse, France

(Received 12 April 2000 and in revised form 6 November 2000)

Optimal perturbations for the family of three-dimensional boundary layers described by the Falkner–Skan–Cooke similarity solution are obtained using a variational technique in the temporal framework. The disturbances experiencing the most growth take the form of vortices almost aligned with the external streamline at inception and evolve into streaks. In subcritical flows these can attain about twice the transient amplification observed in comparably forced two-dimensional flows. Possible connections between optimal perturbations and exponentially amplified crossflow vortices are explored.

---

## 1. Introduction

The laminar–turbulent transition process in boundary layers is generally studied for the limiting case of a two-dimensional base flow. While the complexity of the transition phenomenon warrants such simplification, it happens that three-dimensional boundary layers predominate in a wide spectrum of engineering applications.

The flow over a swept wing is a canonical example of a three-dimensional boundary layer which is of obvious interest to the aerodynamicist. A spanwise pressure gradient on the wing causes a crossflow velocity component to develop inside the boundary layer, altering the flow's stability characteristics as a consequence. In a two-dimensional boundary layer a favourable pressure gradient delays transition by changing the shape of the mean velocity profile. Since laminar flow incurs significantly less viscous drag than turbulent flow, modern wing sections are often designed to ensure a favourable pressure gradient over a large part of the wing chord. It is precisely in this environment, however, that crossflow instability is likely to arise.

Crossflow instability, which came to light in a series of flight tests on swept-wing aircraft by Gray (1952), differs fundamentally from the viscous Tollmien–Schlichting instability occurring in two-dimensional boundary layers, as explained by Gregory, Stuart & Walker (1955). It is an inviscid instability resulting from the inflectional crossflow velocity profile, and manifests itself primarily in the form of steady crossflow vortices almost aligned with the free stream upon which travelling disturbances may be superposed.

A plausible scenario for crossflow-induced transition in the low-disturbance environment likely to be encountered by a cruising commercial airliner can be pieced

† Present address: Institut de Mécanique des Fluides de Toulouse, Allée du Pr. Camille Soula, F-31400 Toulouse, France.

together from the literature. Sub-micron-sized imperfections on the wing surface serve as seed sites for the first identifiable disturbances in the boundary layer, as shown by Radeztsky, Reibert & Saric (1999). These have shapes and wavelengths consistent with the most amplified steady and travelling perturbations predicted by classical stability theory. By all accounts, the major discrepancy between theory and observation lies in quantification of the disturbance's growth rate. Theory predicts that travelling perturbations grow quicker than their steady counterparts, which is precisely the opposite of what is observed in many experiments. This may be explained by observing that the steady vortices are continually excited by surface irregularities, whereas nonlinear interaction at second order in perturbation theory is necessary to generate travelling waves of the correct phase speed. Consequently, as remarked by Reed & Saric (1989), steady crossflow vortices generally predominate in the low-turbulence free-flight environment despite receiving suboptimal amplification. Once present in the flow, steady crossflow vortices grow until they saturate at an amplitude on the order of 10% of the base flow. The distorted boundary layer then becomes susceptible to a high-frequency secondary instability which is generally credited with bringing about transition. For a comprehensive discussion of crossflow transition, see Reed & Saric (1989), Reed, Saric & Arnal (1996), Bippes (1999) and the references therein.

The classical approach to hydrodynamic stability outlined in Drazin & Reid (1981) posits the exponential time dependence of small disturbances in the flow under consideration. Hence a positive growth rate implies instability, although it is worth mentioning that the growth rates of primary instabilities commonly encountered in boundary layer flows are small even for the 'strongly unstable' crossflow instability. Left unclear are two issues of some significance: the first of these is how the boundary layer selects and amplifies arbitrary initial disturbances from the surrounding environment (the so-called 'receptivity' problem); secondly, once this selection has taken place how long does it take for the known instability to establish itself? A very weakly amplified mode may not attain full development until some point past transition. Secondary stability theory, extensively applied in theoretical investigations of crossflow instability, is not exempt from these considerations since it treats the stability of the mean boundary layer flow modified by finite-amplitude disturbances, usually saturated primary instabilities.

So ample motivation exists for investigating mechanisms capable of effecting rapid transient growth. One such mechanism through which three-dimensional disturbances in a mean shear flow can experience at least linear amplification in time has been described by Ellingsen & Palm (1975) and Landahl (1980). This algebraic growth mechanism produces streaks, or large variations in streamwise perturbation velocity, which are pervasive features in transitional boundary layers. The eventual decay of the initial disturbance through viscous diffusion gives the phenomenon its name of 'transient growth'. From the mathematical point of view the transient behaviour of small perturbations in the boundary layer is a consequence of the non-normality of the linearized equations which govern them, as discussed by Trefethen *et al.* (1993).

Recent studies of subcritical two-dimensional boundary layers have shown that disturbances which experience maximum transient amplification exploit this mechanism (see Butler & Farrell 1992; Luchini 1996; Andersson, Berggren & Henningson 1999; Luchini 2000; Corbett & Bottaro 2000). After the work of Butler & Farrell (1992) such configurations of the initial perturbation velocities are termed optimal perturbations (in the sense that they produce the most effect for the least effort). It is not uncommon for the perturbation kinetic energy of optimally initiated disturbances

to increase by several orders of magnitude, even in subcritical flows. Study of optimal perturbations is warranted because they embody the ‘worst-case’ input to the flow on the one hand, and may provide a link to events upstream of the point where an asymptotic state can be said to exist on the other.

Optimal perturbations are of particular interest in swept wing flows since they bear a strong resemblance to the primary exponential instability, in contrast to the two-dimensional case. Thus, at subcritical conditions the algebraic mechanism may actually precondition the boundary layer for the exponential instability which develops later. In a related vein, when the primary instability is triggered optimally it undergoes explosive transient growth, experiencing instantaneous growth rates an order of magnitude larger than asymptotic. These considerations may have some bearing on ‘bypass transition’ scenarios traditionally attributed to nonlinear effects.

Breuer & Kuraishi (1994) have shown that three-dimensional boundary layers are capable of sustaining substantial transient growth. They chart the effects of sweep angle, pressure gradient and Reynolds number on the growth of individual Fourier modes but make no attempt to determine optimal perturbations, choosing to work instead with modified eigenfunctions of the linear stability problem in which the normal vorticity is set to zero. They also limit themselves to relatively large streamwise wavenumbers, citing difficulties in resolving the degenerate discrete spectrum which develops as the streamwise wavenumber tends to zero, even though their results show that most growth occurs in this limit. Hultgren & Gustavsson (1981) have associated the continuous spectrum with transient growth.

In this work optimal perturbations obtained using a temporal approach are presented for the Falkner–Skan–Cooke class of swept boundary layers. The optimization technique is described in terms of a Lagrange multiplier formalism. Subcritical and linearly unstable flows are investigated, and transient growth is found to play a potential rôle in both stability régimes.

The temporal framework and its accompanying parallel-flow assumption comprise this work’s major weakness, although recent results indicate that transients obtained via temporal analysis may be mapped into a spatial context (Meyer 1989; Breuer & Kuraishi 1994; Lasseigne *et al.* 1999). While this lends the present results a preliminary flavour, it should be pointed out that extending the analysis to the more physical spatial framework is not straightforward. An advantage to the temporal approach is that it permits the consideration of oblique disturbances, i.e. flow structures with a streamwise periodicity comparable to the spanwise periodicity, a scenario not permitted by a boundary layer scaling such as that employed in the studies by Luchini (2000) and Andersson *et al.* (1999) in the spatial framework.

## 2. Swept-wing boundary layer

The boundary layer on an infinite swept wing is modelled here using the two-parameter family of similarity solutions for yawed wedge flows given by Cooke (1950). The first parameter,  $m$ , describes the intensity of the pressure gradient, and the second is the yaw (or sweep) angle  $\Lambda$  which provides a relation between chordwise and spanwise velocities. This model’s principal advantage is that the parameters offer a means of systematically varying the magnitude of the mean crossflow velocity component.

The general situation is illustrated in figure 1, where the wing coordinate system (subscript ‘w’) is such that  $x_w$  lies along the wing chord,  $z_w$  is in the spanwise sense and  $y$  is normal to the surface. The corresponding velocity components inside the boundary

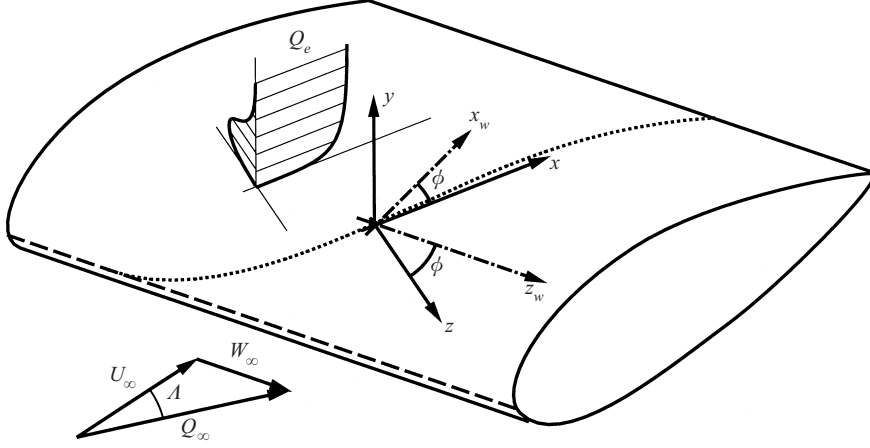


FIGURE 1. Boundary layer development on an infinite swept wing. The attachment line is shown as a dashed line, and the external streamline is indicated by the dotted line. The wing and streamline reference frames are shown, as are the boundary layer velocity profiles in the plane aligned with the external streamline.

layer are  $U_w$ ,  $W_w$  and  $V$ . Using the Blasius similarity variable  $\xi = (U_e/(v x_w))^{1/2} y$ , an affine solution to the boundary layer equations is sought for the case where  $U_e = C x_w^m$  and  $W_e = \text{constant}$ , where the subscript ‘e’ indicates the situation at the boundary layer edge at the chordwise position under consideration. Introducing a stream function of the form  $\psi = (U_e v x_w)^{1/2} f(\xi)$  continuity is satisfied directly, and as a result  $U_w = U_e df/d\xi$ . Assuming  $W_w = W_e g(\xi)$ , the momentum equations then yield the system

$$f''' + \frac{m+1}{2} f f'' + m(1-f^2) = 0, \quad g'' + \frac{m+1}{2} f g' = 0, \quad (2.1a, b)$$

with

$$f(0) = f'(0) = g(0) = 0 \quad \text{and} \quad f'(\infty) = g(\infty) = 1, \quad (2.1c)$$

where primes indicate derivatives with respect to the independent variable. A physically meaningful range of values for the pressure gradient parameter is  $-0.0904 \leq m \leq 1$ , where the lower limit corresponds to imminent separation and the upper limit applies to stagnation-line flows.

After Stuart (Gregory *et al.* 1955, part II), stability is typically studied in the frame of reference of the external streamline. For zero pressure gradient flows the problem reduces to the Blasius case. If  $\phi$  is the angle between the reference frame aligned with the external potential flow and the wing coordinate system, and assuming  $\lambda \approx \phi$  as might be expected some distance from the leading edge, the velocity components parallel and normal to the external flow are given by,

$$U(\xi) = f'(\xi) \cos^2 \phi + g(\xi) \sin^2 \phi, \quad (2.2a)$$

$$W(\xi) = [g(\xi) - f'(\xi)] \cos \phi \sin \phi, \quad (2.2b)$$

when non-dimensionalized with respect to  $Q_e$ , the velocity magnitude at the boundary layer edge.

The effects of the parameters on the base flow can be readily inferred from (2.1) and (2.2). From the widespread appearance of  $m$  in (2.1) it can be appreciated that the pressure gradient plays a strong rôle in determining the shape of both velocity

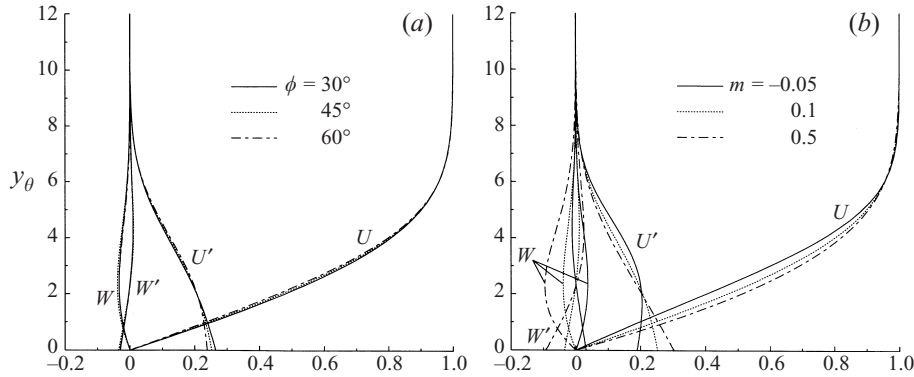


FIGURE 2. Solutions of the Falkner–Skan–Cooke flow, showing (a) the effect of changing  $\phi$  for  $m = 0.1$ , and (b) the effect of varying  $m$  at  $\phi = 45^\circ$ .

$m$	$\phi$ (deg.)	$\delta^*$	$\theta$	$H$	$ W _{\max}$
-0.0904	45	2.9490	0.9370	3.1473	0.1303
-0.05	0	2.1177	0.7515	2.8180	0
	45	2.0042	0.7408	2.7055	0.0373
0.1	0	1.3478	0.5566	2.4215	0
	45	1.4444	0.5806	2.4878	0.0392
	48.8	1.4574	0.5834	2.4981	0.0388
0.46	46.9	1.0734	0.4532	2.3685	0.0927
1	45	0.8371	0.3648	2.2947	0.1199

TABLE 1. Integral boundary layer parameters for selected Falkner–Skan–Cooke profiles.

profiles. At a given pressure gradient, it is clear from (2.2) that the sweep angle will regulate the magnitude, but not the shape, of the mean crossflow. The relationship is investigated further in figure 2, where part (a) shows the retarding effect of increased sweep on  $U$ , and the symmetry of  $W$  about a maximum at  $45^\circ$ . Figure 2(b) presents the result of varying the pressure gradient at fixed sweep; of note here is that the mean crossflow reverses sense when subjected to an adverse pressure gradient.

As is customary, the displacement and momentum thicknesses are defined using only the streamwise velocity component,

$$\delta^* = \int_0^\infty (1 - U) dy \quad \text{and} \quad \theta = \int_0^\infty U(1 - U) dy.$$

For a given pressure gradient, these become weak functions of the sweep angle. Some representative numerical values of these quantities, their ratio in the form of the shape factor  $H$ , and the maximum value of the mean crossflow component are given in table 1.

### 3. Small disturbances

Of interest is the behaviour of a small unsteady three-dimensional perturbation with velocity components  $\tilde{\mathbf{u}}(x, y, z, t) = (\tilde{u}, \tilde{v}, \tilde{w})^T$  in a steady incompressible parallel

boundary layer with crossflow, whose velocity components  $\mathbf{U}(y) = (U, 0, W)^T$  are given by the Falkner–Skan–Cooke similarity solution. Linearizing the Navier–Stokes equations eliminating the pressure and introducing the wall-normal perturbation vorticity,  $\tilde{\eta} = \partial\tilde{u}/\partial z - \partial\tilde{w}/\partial x$ , it becomes possible to describe the perturbation in terms of  $\tilde{\mathbf{v}} = (\tilde{v}, \tilde{\eta})^T$ . Further assuming periodicity of the form

$$\tilde{\mathbf{v}}(x, y, z, t) = \mathbf{v}(y, t) \exp(i\alpha x + i\beta z),$$

where  $\alpha$  and  $\beta$  are real wavenumbers in the stream- and spanwise directions, yields the following system for  $\mathbf{v}$  (which may on occasion be referred to as the ‘state’):

$$\left[ \left( \frac{\partial}{\partial t} + i\alpha U + i\beta W - \frac{1}{R} \Delta \right) \Delta - i\alpha \frac{d^2 U}{dy^2} - i\beta \frac{d^2 W}{dy^2} \right] \mathbf{v} = 0, \quad (3.1a)$$

$$\left( \frac{\partial}{\partial t} + i\alpha U + i\beta W - \frac{1}{R} \Delta \right) \eta = \left( i\alpha \frac{dW}{dy} - i\beta \frac{dU}{dy} \right) \mathbf{v}. \quad (3.1b)$$

Above,  $\Delta = \partial^2/\partial y^2 - k^2$  represents the Laplacian operator, and  $k^2 = \alpha^2 + \beta^2$ . The disturbance evolves from an initial condition  $\mathbf{v}_o(y) = (v_o, \eta_o)^T$  (occasionally termed the ‘control’) which satisfies the boundary conditions, which are as follows: the normal perturbation velocity and its normal derivative vanish at solid walls, and die out in the free stream. Since the stream- and spanwise perturbation velocities also vanish at these boundaries, the normal disturbance vorticity must too.

The Reynolds number, characterizing the relative importance of convective to diffusive processes,

$$R = \frac{Q_e \delta}{\nu},$$

appears when the original system is uniformly non-dimensionalized using a characteristic length ( $\delta$ ) and velocity ( $Q_e$ ). Pressure is scaled by the grouping  $\rho Q_e^2$  and  $\delta$  is taken to be proportional to the boundary layer thickness defined by  $\delta = (\nu \ell / Q_e)^{1/2}$ , where  $\ell$  is a reference distance in the chordwise direction.

A perturbation’s intensity at a given time  $t = \tau$  is typically quantified by its kinetic energy density, defined as

$$E_\tau = \frac{1}{2} \int_0^\infty (\bar{u} \cdot u + \bar{v} \cdot v + \bar{w} \cdot w) dy = \frac{1}{2k^2} \int_0^\infty (-\bar{v} \cdot \Delta v + \bar{\eta} \cdot \eta) dy,$$

where the overbars indicate transpose conjugate quantities. The rightmost term in the expression is found easily after expressing  $u$  and  $w$  in terms of  $v$  and  $\eta$ , and integrating once by parts. Provided the inner product between two arbitrary complex vectors  $\mathbf{p}$  and  $\mathbf{q}$  is defined  $(\mathbf{p}, \mathbf{q}) = \int_0^\infty (\bar{\mathbf{p}} \cdot \mathbf{q}) dy + \text{c.c.}$  with c.c. denoting complex conjugate,  $E_\tau$  is seen to be simply one quarter of the inner product of  $\mathbf{u}(y, \tau)$  with itself. In the discussion to follow importance is attached to disturbances which undergo significant relative amplification over a given time interval. This gain is quantified by the growth, defined as

$$G(\tau) = \frac{E_\tau}{E_o},$$

where  $E_o$  is the kinetic energy density of the initial condition.

In closing this section, note that (3.1) can be written more compactly as,

$$\mathbf{F} \mathbf{v} = 0, \quad \text{where} \quad \mathbf{F} = \mathbf{I} \frac{\partial}{\partial t} + \mathbf{A}. \quad (3.2)$$

In the above expression  $\mathbf{I}$  is the identity matrix and,

$$\mathbf{A} = \begin{bmatrix} \Delta^{-1}(\mathbf{C}\Delta - i\alpha U'' - i\beta W'') & 0 \\ -i\alpha W' + i\beta U' & \mathbf{C} \end{bmatrix}, \quad \text{with } \mathbf{C} = i\alpha U + i\beta W - \frac{1}{R}\Delta.$$

An explicit statement that the state at  $t = 0$  is constrained to match the control,

$$\mathbf{H}(\mathbf{v}(y, 0), \mathbf{v}_o(y)) = (\mathbf{I}, -\mathbf{I}) \cdot (\mathbf{v}(y, 0), \mathbf{v}_o(y))^T = \mathbf{v}(y, 0) - \mathbf{v}_o(y) = 0,$$

will prove useful later on. It is clear that the linearized dynamical operator  $\mathbf{A}$  is not self-adjoint whenever  $\alpha$  and  $\beta$  are not simultaneously zero, i.e. in all cases of physical interest. The implication is that while the long-term behaviour of an arbitrary initial condition is adequately described by a single eigenmode, a short-term transient bearing little resemblance to the mode is possible (Trefethen *et al.* 1993).

#### 4. Optimal perturbations

Optimal perturbations are initial conditions which excite the most energetic perturbation in a given base flow. As remarked by Farrell (1988), ‘the concept of an optimum requires a measure’; this work follows his lead in using the appropriately scaled perturbation kinetic energy density (growth) to gauge optimality. It remains to devise a technique which can be used to determine these optimal initial conditions.

A common approach is to represent generic disturbances as a weighted sum of eigenvectors to the Orr–Sommerfeld/Squire system of equations ((3.1) with exponential time dependence, see §5). The optimization problem then lies in determining the weights which maximize the gain over a given time span, leading to a generalized eigenvalue problem. Butler & Farrel (1992) use this method in their study of optimal perturbations for Couette, Poiseuille and Blasius boundary layer flows, and its use is widespread (Reddy & Henningson 1993; Hanifi & Henningson 1998). A primary inconvenience with this approach is the treatment of the continuous spectrum which plays an important part in transient growth (Hultgren & Gustavsson 1981; Breuer & Kuraishi 1994), particularly as the streamwise wavenumber goes to zero. Further, since the eigenvectors are non-orthogonal, a large number of modes may be required to adequately resolve an arbitrary disturbance.

These problems have inspired the use of alternative vector bases (Lasseigne *et al.* 1999; Cossu *et al.* 2001), although this approach is considerably more involved. The first challenge lies in finding a suitable set of basis functions which is well-adapted to the problem geometry. This is a non-trivial problem in its own right for the case of the semi-infinite boundary layer domain. Then the temporal evolution of each basis function must be determined, before turning to the problem of determining the weight on each basis function, as above.

An efficient variational alternative has been used by Luchini & Bottaro (1998), Andersson *et al.* (1999), Luchini (2000) and Corbett & Bottaro (2000). The usual description of this technique centres on the definition for  $G$  and the inner product defining the energy. Upon introducing the propagator, the evolution operator which takes an initial condition  $\mathbf{v}_o$  to the state at  $t = \tau$ , it becomes possible to form a Rayleigh quotient in which the adjoint to (3.1) under the energy inner product appears. This is amenable to solution via power iteration (for an elegant account, see Luchini 2000).

The mathematical framework of optimal control theory can also be employed to find optimal perturbations. The essential elements in an optimal control problem are a mathematical description of the objective to be attained, some means of adjusting

the system to meet the objective, and a description of the system and its behaviour (Abergel & Témam 1990; Gunzburger 2001). The last element (the constraints) is provided by (3.1) and its boundary conditions, which together describe the state of the perturbation at any instant in time. The second element (the control) is furnished by the initial conditions  $\mathbf{v}_o$  through which the state can be directly affected. Finally, a suitable real objective functional over the time interval  $t = \tau$  is simply the growth,

$$\mathcal{J}(\mathbf{v}, \mathbf{v}_o) = G(\tau).$$

Formally, the task is now to maximize  $\mathcal{J}$ , a proposition which is considerably complicated by the constraints on the state and the control.

In the light of the difficulties inherent in constrained optimization it is convenient to introduce the adjoint (or costate) variables,  $\mathbf{a}(y, t) = (a, b)^\top$  and  $\mathbf{c}(y) = (c, d)^\top$ , and to write a Lagrangian functional,

$$\mathcal{L}(\mathbf{v}, \mathbf{v}_o, \mathbf{a}, \mathbf{c}) = \mathcal{J} - \langle \mathbf{F}\mathbf{v}, \mathbf{a} \rangle - \langle \mathbf{H}, \mathbf{c} \rangle, \quad (4.1)$$

where the adjoint quantities play the rôle of Lagrange multipliers in enforcing the constraints. Again  $\mathcal{L}$  is exclusively real, and the new inner product appearing above is defined  $\langle \mathbf{p}, \mathbf{q} \rangle = \int_0^\tau \int_0^\infty (\bar{\mathbf{p}} \cdot \mathbf{q}) \, dy \, dt + \text{c.c.}$ , ensuring that the range of the functional is the real line. Since they have not been enforced with their own Lagrange multipliers, all candidate solutions will furthermore be required to satisfy the original system's boundary conditions.

The introduction of the Lagrangian functional replaces the original constrained optimization problem for  $\mathcal{J}$  with an equivalent unconstrained problem for  $\mathcal{L}$ . Now the task is to determine  $\mathbf{v}$ ,  $\mathbf{v}_o$ ,  $\mathbf{a}$  and  $\mathbf{c}$  which render  $\mathcal{L}$  stationary, in accordance with the first-order necessary conditions for an extremal point. This is accomplished by setting to zero the directional derivative with respect to an arbitrary variation in the variable under consideration, e.g. in the case of the state,

$$\frac{\partial \mathcal{L}}{\partial \mathbf{v}} \delta \mathbf{v} = \lim_{\varepsilon \rightarrow 0} \frac{\mathcal{L}(\mathbf{v} + \varepsilon \delta \mathbf{v}, \mathbf{v}_o, \mathbf{a}, \mathbf{c}) - \mathcal{L}(\mathbf{v}, \mathbf{v}_o, \mathbf{a}, \mathbf{c})}{\varepsilon},$$

where in contrast to the case of the constrained functional, each of the arguments of  $\mathcal{L}$  is considered to be an independent variable. It must be stressed that this approach provides a local extremum, with no guarantee that it happens to be a global extremum.

Setting the first variation of the Lagrangian with respect to the state variables to zero as indicated above is greatly simplified provided the adjoint under the bracket inner product is employed. By definition this is  $\langle \mathbf{v}, \mathbf{F}^* \mathbf{a} \rangle$  where the adjoint operator is expressed compactly as  $\mathbf{F}^*$  in analogy to (3.2). Moving  $\mathbf{F}$  to the other side of the inner product involves repeated integration by parts, giving rise to terms which define the boundary conditions on  $\mathbf{F}^*$ . In this manner equations for the costate are obtained,

$$\left[ \left( \frac{\partial}{\partial t} + i\alpha U + i\beta W + \frac{1}{R} \Delta \right) \Delta + 2i \left( \alpha \frac{dU}{dy} + \beta \frac{dW}{dy} \right) \frac{\partial}{\partial y} \right] a = \left( i\alpha \frac{dW}{dy} - i\beta \frac{dU}{dy} \right) b, \quad (4.2a)$$

$$\left( \frac{\partial}{\partial t} + i\alpha U + i\beta W + \frac{1}{R} \Delta \right) b = 0, \quad (4.2b)$$

where the boundary conditions on  $\mathbf{a}$  are identical to those for  $\mathbf{v}$ . Additionally, from



(3.1a) one has

$$-\frac{1}{2k^2 E_o} \Delta v(y, \tau) = \Delta a(y, \tau), \quad \text{and} \quad \Delta a(y, 0) = c(y);$$

and from (3.1b),

$$\frac{1}{2k^2 E_o} \eta(y, \tau) = b(y, \tau), \quad \text{and} \quad b(y, 0) = d(y).$$

Enforcing stationarity with respect to variations in the control,  $(\partial \mathcal{L} / \partial \mathbf{v}_o) \delta \mathbf{v}_o = 0$ , yields the optimality conditions,

$$-\frac{E_\tau}{2k^2 E_o^2} \Delta v_o(y) = c(y), \quad \text{and} \quad \frac{E_\tau}{2k^2 E_o^2} \eta_o(y) = d(y).$$

Finally, it is immediately evident upon setting the first variation of the Lagrangian with respect to the adjoint variables to zero,  $(\partial \mathcal{L} / \partial \mathbf{a}) \delta \mathbf{a} = 0$  and  $(\partial \mathcal{L} / \partial \mathbf{c}) \delta \mathbf{c} = 0$ , that one recovers the constraint equations, completing the optimality system. The above expressions are identical to those obtained from the Rayleigh quotient approach referred to previously, although the manner in which they come about is different. Notably, the system of adjoint equations under the bracket inner product turns out to be identical to the adjoint under the energy inner product appearing in the Rayleigh quotient approach.

Combining the last series of results provides transfer relations between the direct and adjoint systems at time  $t = \tau$ ,

$$a(y, \tau) = -\frac{1}{2k^2 E_o} v(y, \tau), \quad b(y, \tau) = \frac{1}{2k^2 E_o} \eta(y, \tau), \quad (4.3a, b)$$

as well as an expression for the optimal perturbation,

$$v_o(y) = -\frac{2k^2 E_o^2}{E_\tau} a(y, 0), \quad \eta_o(y) = \frac{2k^2 E_o^2}{E_\tau} b(y, 0). \quad (4.4a, b)$$

Implicit within these relations is the iterative algorithm used to find the optimal perturbation. A guess is made for  $\mathbf{v}_o$  and (3.1) is integrated to  $t = \tau$ . Using (4.3), this result provides appropriate terminal conditions for (4.2) which is marched backwards in time to  $t = 0$ , where (4.4) gives an improved set of initial conditions for the next iteration. Convergence using this simple iterative approach (equivalent to using a steepest descent method for  $\mathcal{J}$ ) is quite rapid, rendering more sophisticated algorithms unnecessary. In practice it is uncommon to perform more than five iterations to obtain a converged result, which serves as an *a posteriori* indicator that the first two singular values of the propagator are well separated, see §6. (Convergence is attained when the  $L_2$  norm of successive iterates for  $\mathbf{v}_o$  differ by less than  $10^{-4}$ , i.e.  $\mathcal{J}$  changes less than  $10^{-9}$ .) The fact that the procedure only guarantees a local extremum of the objective functional is tempered by the observation that it will converge to the singular vector corresponding to the largest singular value unless this happens to be perfectly orthogonal to the arbitrary initial guess. The large separation between the first and second singular values serves as a check on the worst-case scenario, easily remedied by choosing another starting point.

## 5. Numerical treatment

The spatial discretization of (3.1) and (4.2) is accomplished using a Chebyshev collocation technique, whereas the temporal discretization is carried out using second-

order backward Euler finite differences (Canuto *et al.* 1988). The computational space, in which the unknowns are represented at the Chebyshev–Gauß–Lobatto nodes  $\zeta$ , is mapped into the physical domain using an algebraic mapping  $y = y_\infty(h/2)(1+\zeta)/(1+h-\zeta)$ , where  $h$  is a constant stretching factor and  $y_\infty$  is the location of the upper boundary. Derivatives are obtained via matrix-vector multiplication with the differentiation matrix, which is suitably adjusted by the Jacobian of the mapping. Integral quantities are obtained using similarly adjusted Gaussian quadrature rules, and are efficiently computed as vector products. The problem is programmed in Matlab, and the collocation points and derivative matrices are computed using the DMSuite package by Weideman & Reddy (2000). Time advancement requires a matrix-vector multiplication and storage for two previous solutions.

Numerical parameters have been determined by grid convergence study. All data presented have been obtained using  $n = 93$  collocation points,  $\delta t \leq 0.2$ , and  $y_\infty = 100$  (based on  $\delta$ ). A value of  $h = 1/9$  has been used for the stretching factor, placing half the points inside the boundary layer.

Optimizations with respect to two or more parameters have been performed using the Nelder–Mead simplex algorithm (Press *et al.* 1992); results are verified using different initial guesses. When optimizing with respect to one parameter, a line search algorithm based on golden section search and parabolic interpolation has been employed.

Modal results are easily obtained by assuming exponential time dependence,

$$\mathbf{v}(y, t) = \hat{\mathbf{v}}(y) \exp(-i\omega t),$$

where the angular frequency  $\omega$  is complex. Then from (3.2) one obtains the Orr–Sommerfeld/Squire system,

$$\mathcal{A}\hat{\mathbf{v}} = i\omega\hat{\mathbf{v}},$$

which is a generalized eigenproblem and can be efficiently inverted using the QZ algorithm.

## 6. Results

It is desirable to quantify the transient growth possible in three-dimensional boundary layers, and to compare it to that occurring in similar two-dimensional flows. The algebraic instability of Falkner–Skan flows has been considered in a previous study by Corbett & Bottaro (2000), and those results will be employed for comparison purposes. Since the Falkner–Skan–Cooke boundary layer only engenders a crossflow component for non-zero pressure gradient and sweep, confirmation will be sought that the effects of the pressure gradient are the same in two- and three-dimensional base flows; and the nature of the effect (if any) the sweep angle has on the transient growth will be determined. Lastly, because the exponential crossflow instability and the lift-up mechanism responsible for transient growth in two-dimensional flows are both inviscid in nature and resemble one another physically, it is natural to explore possible links between these mechanisms.

### 6.1. Terminology

In the temporal framework, an optimal perturbation is defined with respect to a given lapse of time. Consider a subcritical mean flow parameterized by  $R$ ,  $m$  and  $\phi$ . Of all initial conditions  $v_o$  described by the wavenumber pair  $(\alpha, \beta)$ , an optimal perturbation for the finite period  $t = \tau$  attains the largest possible growth over that time span,

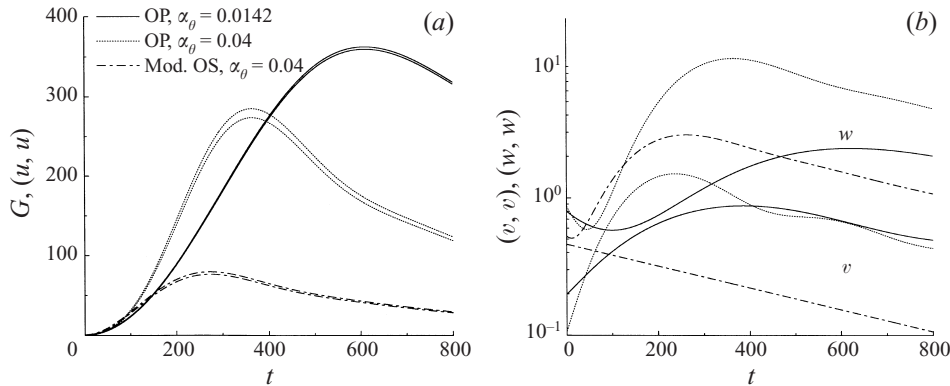


FIGURE 3. Comparison of the growth attained by different initial conditions at  $R_\theta = 166$ ,  $m = 0.1$ ,  $\phi = 48.8^\circ$  and  $\beta_\theta = 0.2327$ . Optimal perturbations are denoted OP. (a) The total growth and (slightly smaller) contribution from the streamwise velocity alone; (b) contributions from perturbation velocities in the crossflow plane.

$G(\tau) = G(R, m, \phi, \alpha, \beta, \tau)$ . What is referred to here as a global optimal perturbation is the combination of initial conditions and time span which together produce the largest possible growth for all times,

$$\gamma = G(t_\gamma) = \max_{\forall t} G(R, m, \phi, \alpha, \beta, t),$$

where  $t_\gamma$  denotes the interval on which this growth is attained.

In flows where exponential amplification is possible, global growth for unstable perturbations is unbounded. Optimal perturbations for finite intervals can still be determined, however, and here these will be referred to as local or short-term optimals. As the interval under consideration increases beyond the duration of the transient event, the asymptotic state sets in and the optimal perturbation for the modal mechanism is recovered. As shown by Hill (1995), in this case the form of the optimal is given by the eigenvectors to the adjoint stability problem which comes about when the solution to (4.2) is assumed to have exponential time dependence.

## 6.2. Previous work

Breuer & Kuraishi (1994) have investigated transient phenomena in Falkner–Skan–Cooke flows, demonstrating that these can support appreciable growth. They integrate (3.1) using ‘near-optimal’ initial conditions, constructed by setting the normal vorticity of the least damped Orr–Sommerfeld (OS) eigenfunction to zero. For numerical reasons, they restrict themselves to modes with  $\alpha_\theta \geq 0.04$ . To justify the more involved procedure outlined in §4, it suffices to compare the growth obtained by such a modified mode and that experienced by a global optimal perturbation for the same conditions, as shown in figure 3. The same figure presents results for a global optimal with a streamwise wavenumber approximately one-third of the others, but the same spanwise wavenumber. The full details for these three cases are reported in table 2. Note that all results in this work are presented scaled in terms of the momentum thickness, which was shown to be the most appropriate scaling for Falkner–Skan flow by Corbett & Bottaro (2000).

The previous example argues that determining true optima is a worthwhile exercise: not only do they experience substantially more growth than modified OS modes, but this growth occurs for perturbations of small streamwise wavenumber, which pose no

---

$\alpha_\theta$	$\beta_\theta$	$\gamma$	$t_\gamma$
0.0142	0.2327	361.9	608.7
0.04	0.2327	284.9	363.5
0.04	0.2327	79.7	272.6

---

TABLE 2. Maximum transient growth parameters for  $R_\theta = 166$ ,  $m = 0.1$ ,  $\phi = 48.8^\circ$ . The first two entries report growth experienced by optimal perturbations, the last entry records that obtained by the least-damped Orr–Sommerfeld mode with  $\eta$  set to zero.

difficulty for the procedure of §4. As might be expected from boundary layer scaling, the streamwise velocity component of the perturbation is the prime benefactor from algebraic amplification, and while the normal velocity is a driving factor in the process, its magnitude contributes the least to the overall growth. However, in contrast to the modified OS mode in which the normal perturbation velocity decays directly, optimal perturbations are configured so that it also undergoes a transient, peaking before the maximum growth is obtained. After the growth phase in this subcritical boundary layer all disturbances decay at the rate of the asymptotic state predicted by classical theory.

The velocity profiles of the three disturbances just discussed are given in figure 4. Parts (a) and (b) show the initial conditions and are scaled to unit normal velocity. The most evident difference between the optimals and the modified OS mode is in the crossflow-plane velocity components; it is worthwhile mentioning in this regard that the normal perturbation vorticity of optimal perturbations is small, but non-zero. Parts (c) and (d) of the figure show the disturbances as maximum growth is attained; here the scaling is to unit streamwise velocity. The output states are remarkably similar, particularly for the case in which the wavenumbers are identical, despite the differing initial conditions. As is the case for two-dimensional boundary layers, the overall end state is a streak, and the input crossflow vortex is on the verge of undergoing viscous dissipation, cf. figure 3.

Luchini (2000) has shown that it is the structure of the singular-value spectrum of the propagator which is responsible for driving sub-optimal initial conditions to output states that are close to optimal. He observes that the effect of the evolution operator is equivalent to expanding an arbitrary initial condition as a weighted sum of the operator’s left singular vectors, and then replacing these with the right singular vectors, adjusting the corresponding weights in the sum by the singular values. Provided that the growth (or first singular value) is substantially larger than all other singular values, it follows that the output state of any initial condition will strongly resemble that resulting from the optimal perturbation.

### 6.3. Effect of three-dimensionality

An idea of the extent and magnitude of transient growth possible in a given flow is rapidly obtained by considering a plot of level curves of  $\gamma$  and  $t_\gamma$  in the wavenumber plane. Figures 5 and 6 present this information for swept and unswept Falkner–Skan–Cooke flows subject to adverse ( $m = -0.05$ ) and favourable ( $m = 0.1$ ) pressure gradients. In the three-dimensional case, the sweep angle,  $\phi = 45^\circ$ , is such that the crossflow component of the base flow is maximized. The Reynolds number,  $R_\theta = 166$ , corresponds to that investigated by Corbett & Bottaro (2000), whence the results for the two-dimensional flow originate. The conditions for maximum global growth in these flows are summarized in table 3.

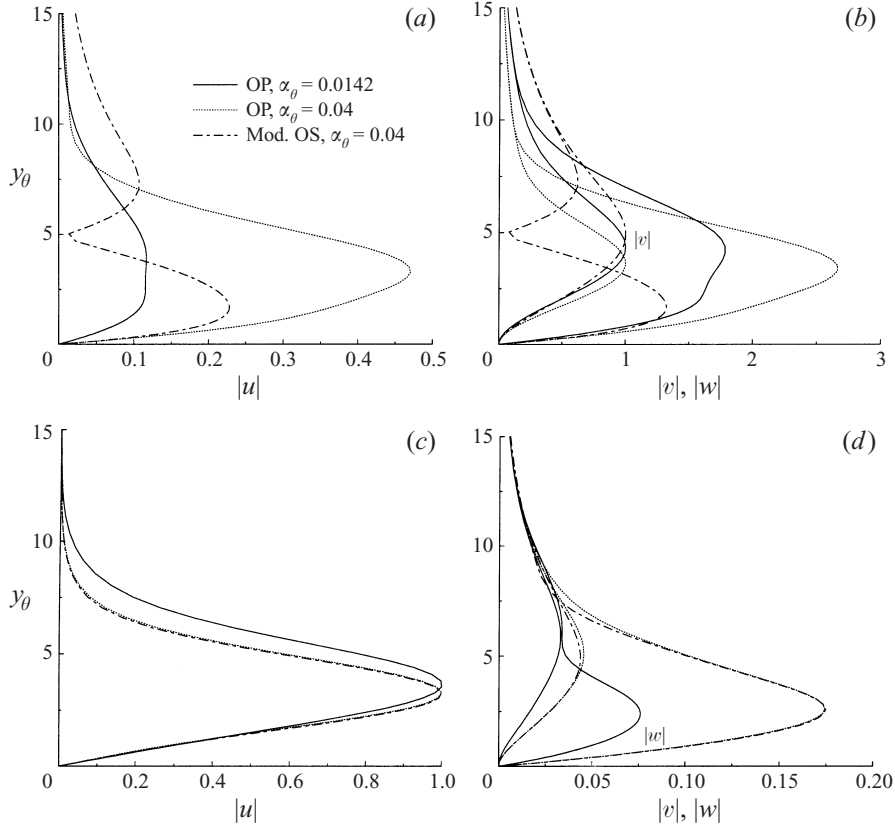


FIGURE 4. Profiles of perturbation velocity magnitude corresponding to the cases in figure 3. (a, b) Initial conditions scaled such that  $|v|_{\max} \equiv 1$ , (c, d) at time of maximum growth, scaling such that  $|u|_{\max} \equiv 1$ . See table 2 for full details.

---

$m$	$\phi$ (deg.)	$\alpha_\theta$	$\beta_\theta$	$\gamma$	$t_\gamma$
-0.05	0	0	0.2511	356.4	898.2
	45	-0.0179	0.2449	506.3	590.8
0.1	0	0	0.2522	227.4	863.5
	45	0.0140	0.2312	360.0	616.0

---

TABLE 3. Characteristics of the maximum global optimals for two- and three-dimensional boundary layers at  $R_\theta = 166$ .

The swept boundary layer subject to a moderately adverse pressure gradient portrayed in figure 5(a) illustrates a case where algebraic growth coexists with Tollmien–Schlichting and crossflow instabilities. In this figure, areas of the wavenumber plane which experience exponential amplification are shaded, and the extent of TS instability in the two-dimensional flow is indicated with a dotted line. The region of the wavenumber plane subject to crossflow instability extends from the area dominated by TS instability right into the heart of the area experiencing the largest algebraic growth. In this case the largest transient growth is obtained by a disturbance which lies at a point on the neutral stability curve. Notable is that the swept-wing flow

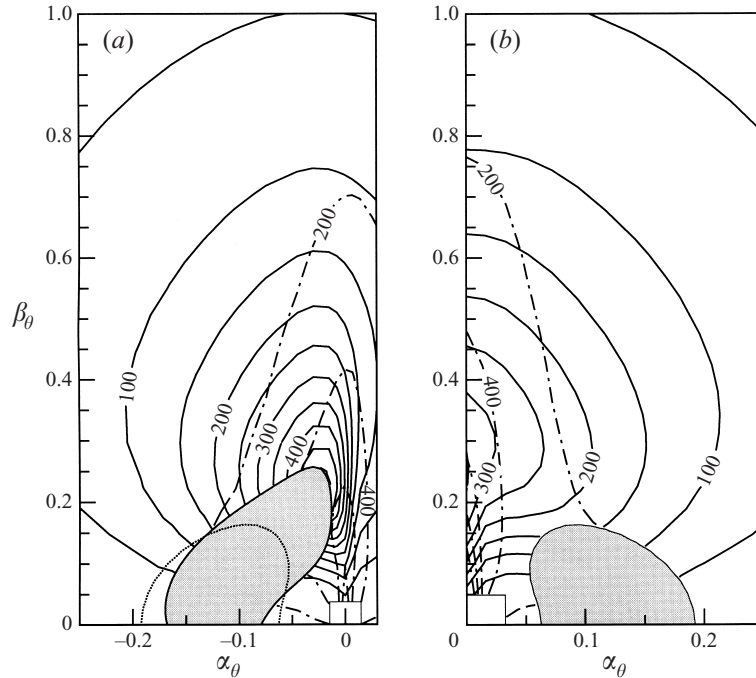


FIGURE 5. (a) Maximum transient growth in a retarded three-dimensional boundary layer: solid lines  $\gamma$ , dash-dot lines  $t_\gamma$ . The flow parameters are  $R_\theta = 166$ ,  $m = -0.05$ ,  $\phi = 45^\circ$ . The shaded region indicates exponential instability, the dotted line represents its extent for two-dimensional flows. (b) Transient growth in a two-dimensional boundary layer subject to an identical pressure gradient (from Corbett & Bottaro 2000).

sustains growth of almost half as much again as its two-dimensional counterpart, in about two-thirds the time.

Figure 6 presents an analogous situation for the accelerated boundary layer, which at this mild pressure gradient and low Reynolds number is entirely subcritical. Again, in comparison to the unswept case the three-dimensional flow sustains significantly more algebraic growth over a shorter time span.

Velocity profiles of the global optimal perturbation responsible for the greatest growth in each of the four flows are reported in figure 7, both at inception and at the time maximum growth is attained. It can be seen that momentum thickness scaling is somewhat less efficacious for three-dimensional boundary layers, but the maximum velocity amplitude remains well correlated. As is customary, the optimal perturbations have been scaled to unit normal velocity, and the output state has been scaled to unit streamwise velocity. The parameters for optimal growth are reported in table 3. In comparison to their two-dimensional counterparts, optimal perturbations in swept boundary layers have larger stream- and spanwise perturbation velocity amplitudes; furthermore the maximum perturbation amplitude is closer to the wall. Especially remarkable is the disparity in size of the initial vortex at the point of maximum amplification between the two classes of flows.

In contrast to the two-dimensional case, the physical mechanism responsible for transient growth is not immediately evident from the perturbation velocity profiles shown in figure 7. To shed more light on the situation, the time evolution of the optimal perturbation for the favourable pressure gradient case is shown in figure 8.

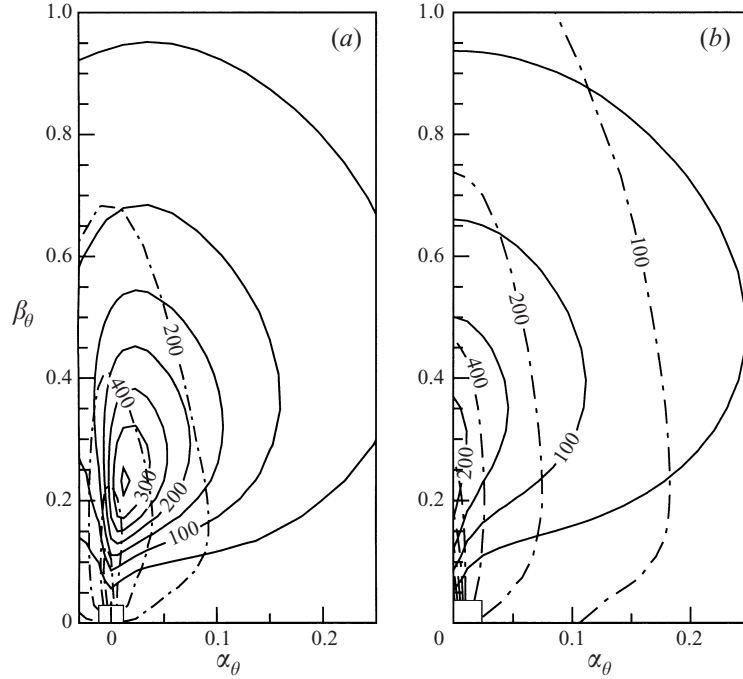


FIGURE 6. (a) Maximum transient growth in an accelerated three-dimensional boundary layer: solid lines  $\gamma$ , dash-dot lines  $t_\gamma$ . The flow parameters are  $R_\theta = 166$ ,  $m = 0.1$ ,  $\phi = 45^\circ$ . (b) Transient growth in a similarly accelerated two-dimensional boundary layer (from Corbett & Bottaro 2000).

It shows snapshots of the optimal perturbation in the crossflow plane, alternating between contours of  $u$  (negative iso-lines are dotted, and zero has been omitted) and a vector representation of the crossflow velocity components of the disturbance, as time increases from left to right. Contours of  $u$  on the plane  $y_\theta \approx 4$  are also shown, from which the rapidity of the growth can be appreciated, as well as the longevity of the streaks produced by the optimal.

#### 6.4. Optimal sweep

To obtain an upper bound on the transient growth possible in a swept boundary layer at given  $R$  and  $m$ , it is necessary to optimize  $\gamma$  with respect to the sweep angle. The result of such an optimization for  $R_\theta = 166$ ,  $m = 0.1$  is shown in figure 9. Part (a) reports the optimal sweep angle  $\Phi$ , i.e.  $\gamma(\Phi) = \max_{\forall \phi} \gamma(\phi)$ ; part (b) shows level curves of  $\gamma$  and  $t_\gamma$  obtained at  $\Phi$ . Since the base flow is a weak function of the sweep angle, a relatively small difference is observed in the growth at conditions of maximum crossflow presented in figure 6(a) and that at the optimal sweep angle.  $\Phi$  is never less than about  $48^\circ$ , and the largest maximum amplification occurs for a flow angle close to this minimum. The shape of the maximum global optimal perturbation at these conditions has already been reported in figure 4; it is quite similar to that found at  $45^\circ$ .

In the wavenumber-plane surveys reported in figures 5, 6 and 9,  $t_\gamma$  is fairly moderate in much of the plane, but experiences a well-defined peak for disturbances characterized by large spanwise wavelength and close to steady in the streamwise sense. No attempt has been made to obtain data for very small wavenumbers since the very long time intervals required for globally optimal growth render the validity

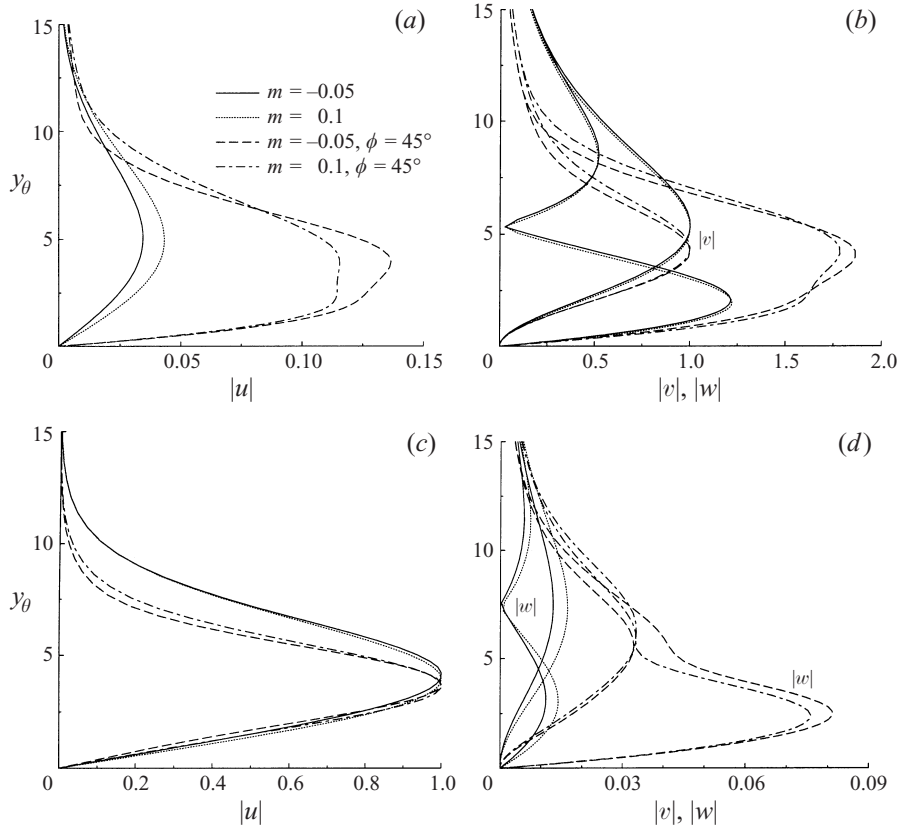


FIGURE 7. Comparison of optimal perturbation velocity profiles for identically accelerated two- and three-dimensional boundary layers. (a, b) Initial conditions, scaled such that  $|v|_{\max} \equiv 1$ . (c, d) Evolved state at  $t_\gamma$ . Scaling here is such that  $|u|_{\max} \equiv 1$ , see table 3 for complete details.

of the parallel flow assumption questionable. For this reason the near vicinity of the origin has been left blank in these plots.

### 6.5. Symmetries

It is noticeable that the level curves of  $\gamma$  and  $t_\gamma$ , as well as the regions of exponential instability shown in figures 5 and 6 are asymmetric for swept boundary layers. This is due to the more complicated source term in (3.1b) when a mean crossflow component is present. While (3.1) is symmetric about the origin when the base flow is two-dimensional, the opposing signs in the source term when  $W \neq 0$  causes it to become skew-symmetric about the origin. From figure 2 one can anticipate that this asymmetry will be mild unless the ratio  $\alpha/\beta$  is quite large; the crossflow derivative will not dominate in the cases considered here unless this ratio is about 5 or larger. The reason why the asymmetry develops differently in the adverse and favourable pressure gradient cases is that the sign of the mean crossflow changes in these two cases.

The situation is different for the optimal flow angle. While the results shown in figure 9(b) are symmetric about the origin, things are more complex for  $\Phi$ , which is skew-symmetric with respect to  $90^\circ$  about the origin. This behaviour is attributable on the one hand to the source term in (3.1b), and on the other to the parity of the base flow



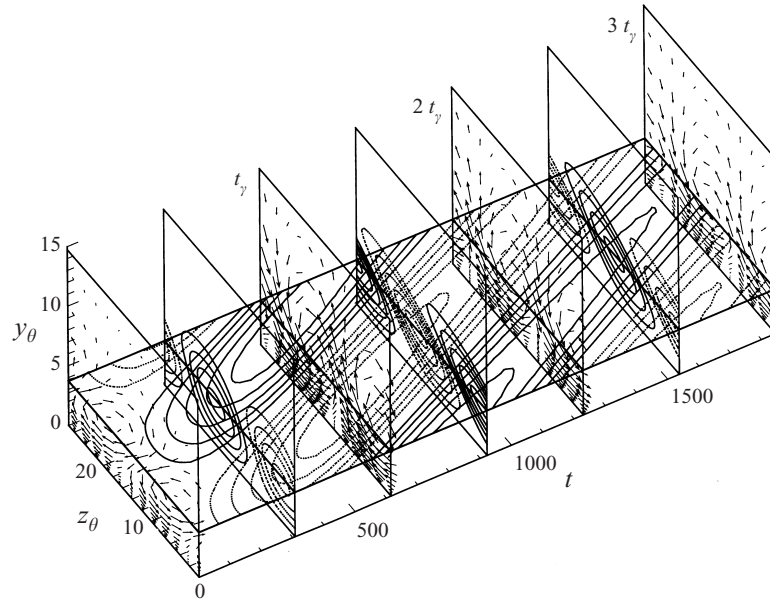


FIGURE 8. Evolution of an optimal perturbation in an accelerated three-dimensional boundary layer illustrating the lift-up effect. An upwelling of near-wall fluid can be observed in correspondence with the axis of the low-speed streak.

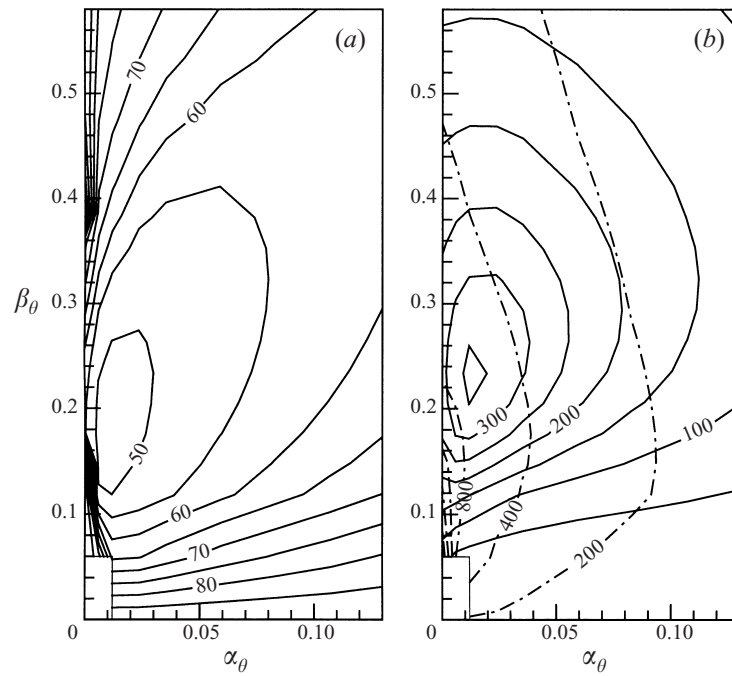


FIGURE 9. The effect of external flow angle on algebraic growth for a flow at  $R_\theta = 166$  and  $m = 0.1$ . (a) Level curves of  $\Phi$ , the sweep angle at which most transient growth occurs. (b) Contours of  $\gamma$  (solid) and  $t_\gamma$  (dash-dot) in a flow so swept.

components:  $U(\phi) = U(180^\circ - \phi)$  is even about  $90^\circ$  whereas  $W(\phi) = -W(180^\circ - \phi)$  is odd.

### 6.6. Algebraic and exponential instability

Above, it has been shown that in contrast to the case of the Falkner–Skan profiles, where the transient growth mechanism competes with the Tollmien–Schlichting instability, in swept boundary layers the algebraic growth mechanism and the exponential crossflow instability are complementary, i.e. both excite disturbances of similar structure (cf. figure 5). In the light of this and the argument that almost any input disturbance will be converted into the final state resulting from optimal perturbation of the flow (Luchini 2000), it is natural to inquire what rôle is played by transient phenomena in flows subject to crossflow instability.

Short-term optimals, or initial conditions which evoke the largest growth at a fixed time  $t = \tau \leq t_\gamma$ , specified by

$$G(\tau) = \max_{\forall \alpha, \beta} G(R, m, \phi, \alpha, \beta, \tau),$$

play a significant part in such an enquiry. This statement is based on the observation that, in the event that temporal results can be transferred to the spatial context by appeal to some  $O(1)$  convection speed, as would seem plausible based on the direct numerical simulation results of Breuer & Kuraishi (1994) in the temporal framework and Lasseigne *et al.* (1999) in the spatial framework, the global optimal perturbation will require a significant streamwise distance of  $O(R\delta)$  to develop fully. The explosive growth over short intervals characteristic of local optima may be especially relevant for flows in which saturation of the primary instability and nonlinear effects are prime causes of transition onset.

Figure 10 presents level curves of  $G$  at  $t = 165.6$  in a strongly accelerated Falkner–Skan–Cooke flow subject exclusively to crossflow instability. The flow conditions correspond to the boundary layer studied extensively at the German Aerospace Centre (DLR) described by Bippes (1999); in particular they correspond to those used in investigations via temporal direct simulation by Meyer (1989) and Meyer & Kleiser (1990):  $R_\theta = 374$ ,  $m = 0.46$  and  $\phi = 46.9^\circ$ . The boundaries of the exponentially unstable regions are indicated by heavy lines. Symbols connected by a dashed line indicate the wavenumber pairs of the perturbations experiencing the most short-term growth at ten equally spaced intervals spanning the transient development time of the optimal perturbation for the most amplified mode, indicated by the solid dot. Noteworthy is that over brief time spans the short-term optima lie outside the exponentially unstable region, that substantial transient growth occurs over a large area of the wavenumber plane, and that at the time shown in the figure the most transient growth at the spanwise wavenumber of the (eventually) most amplified mode is produced for a structure which is exponentially damped.

As mentioned previously, the spanwise wavelength of experimentally observed crossflow vortices concurs well with that of the theoretically most amplified mode, but there are discrepancies concerning the growth rate. The above observation concerning the short-term behaviour of disturbances at identical spanwise wavelengths, but larger streamwise wavenumbers, is explored further in figure 11(a), which presents the growth obtained by the most amplified mode and two other disturbances at integer multiples of its streamwise wavenumber. The first of these is exponentially amplified, the second is not. If one argues that the boundary layer is likely to select disturbances with large instantaneous growth rates, then the observation of disturbances with

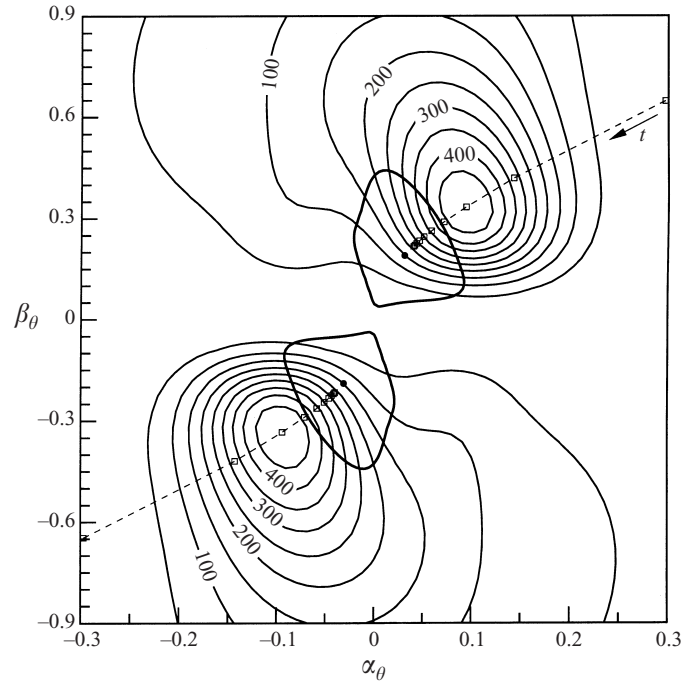


FIGURE 10. Level curves of locally optimum growth for  $t = 165.6$  at DLR conditions. The modally amplified region of the wavenumber plane is enclosed by the thick lines; the wavenumber pairs yielding locally maximum growth for  $t = 55.2, 110.4 \dots 552$  are indicated by the symbols; the wavenumber pair corresponding to the mode with largest growth rate is indicated by the dot.

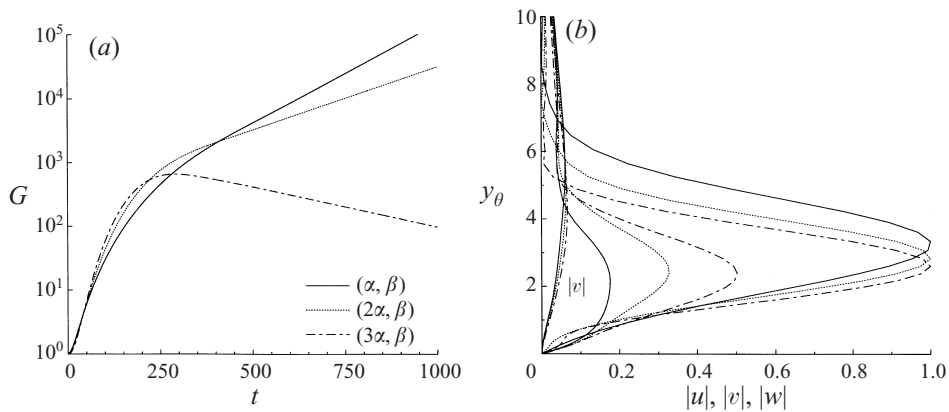


FIGURE 11. (a) Growth exhibited by three optimally excited modes with different streamwise wavelengths but the same spanwise wavelength as the mode with the largest exponential growth rate. (b) Velocity profiles of the corresponding output states, scaled to unit streamwise velocity.

lower than maximum asymptotic growth rates may be explained by their larger initial (and instantaneous) rates of amplification. Figure 11(b) shows the asymptotic disturbance velocity profiles, which are quite similar, apart from the magnitude of the  $w$ -component.

Alternatively, one might consider the state of the boundary layer immediately before it becomes unstable. In the temporal framework this means at a smaller

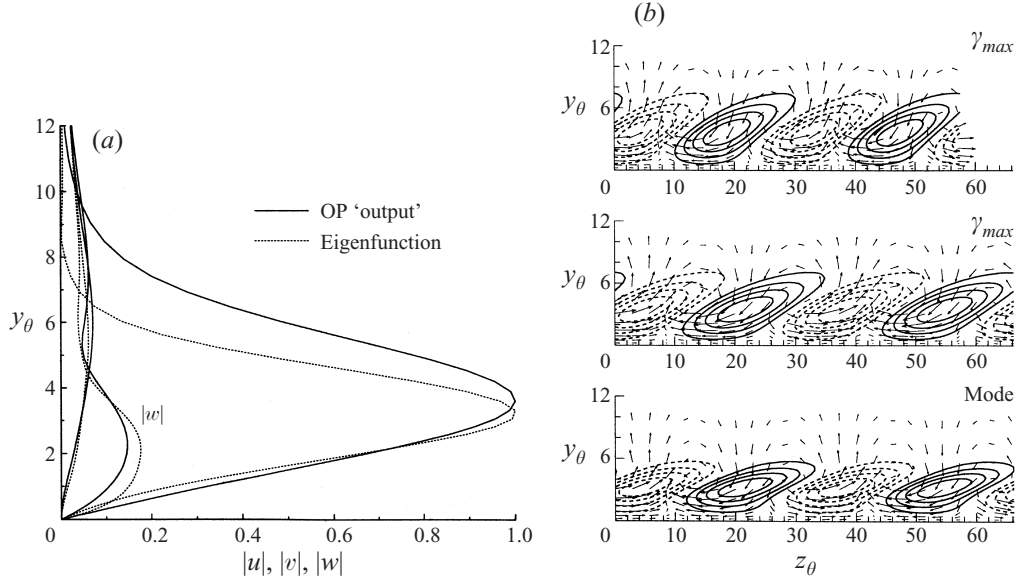


FIGURE 12. (a) Profiles of disturbance velocity magnitude for the most amplified crossflow mode at  $R_\theta = 374$  and the maximum global optimal at  $R_\theta = 91$ . (b) The disturbance fields in (a) projected onto a two period expanse of the crossflow plane. Shown are level curves of  $u$  (dashed negative) and the crossflow velocity components. The uppermost plot corresponds to the maximum global optimum at  $R_\theta = 91$ , the lowermost plot shows the most amplified mode at  $R_\theta = 374$ , and the middle plot shows the global optimal with wavenumbers identical to the mode below, at  $R_\theta = 91$ .

Reynolds number but otherwise identical flow conditions. The reasoning behind this is as follows: the wavenumber pair describing the global optimal with largest growth in subcritical flows is quite similar to that describing the most amplified mode when the boundary layer is unstable. Thus, it seems logical to ask whether the output of the algebraic growth mechanism bears any resemblance to the mode predicted by theory, and which agrees with measurements. Figure 12(a) compares the velocity profiles of the 'output' state of the maximum global optimal perturbation in a subcritical flow at  $R_\theta = 91$  with the eigenfunction of the most amplified mode at  $R_\theta = 374$ . The two sets of profiles are quite similar, indicating that algebraically growing disturbances at low  $R$  are naturally fed into steady crossflow modes as the flow evolves. One could argue that in swept flows algebraic growth preconditions the flow to provide proper initial disturbances to the exponential instability. This is not the case in two-dimensional base flows, where the output of the transient (the streak) bears no resemblance to the modal instability (the TS wave). Figure 12(b) compares reconstructions in the crossflow plane of two optimal perturbations at  $R_\theta = 91$  with the most amplified mode at  $R_\theta = 374$ . The first of the optimals for the subcritical flow is the maximum global optimal, the second is described by the same wavenumber pair as the most amplified mode.

## 7. Concluding remarks

Optimal perturbations, by definition those initial conditions which bring about the largest increase in disturbance kinetic energy, have been studied in quasi-three-dimensional boundary layers modelled by the Falkner–Skan–Cooke similarity sol-

ution. Sub- and supercritical flows subject to adverse and favourable pressure gradients have been considered using a variational technique in the temporal framework. This approach enables disturbances infinitely elongated in the streamwise sense to be studied, impossible with the methods dependent upon some approximation of the continuous spectrum of eigenmodes hitherto employed in investigating this class of flows.

At conditions where only algebraic growth occurs optimal perturbations consist of streamwise oriented vortices which engender a streamwise streak. The vortex/streak axis is not perfectly aligned with the external streamline in which the analysis is performed, i.e. the disturbance has a long (but finite) streamwise wavelength. It is shown that, in comparison to the modified Orr–Sommerfeld modes used by Breuer & Kuraishi (1994), optimal perturbations concentrate more kinetic energy closer to the wall and experience significantly greater growth.

By considering three-dimensional boundary layers at flow conditions comparable to those used in an earlier study of Falkner–Skan flow by Corbett & Bottaro (2000), the effect of crossflow upon transient growth can be determined. At the sweep angle which maximizes crossflow ( $45^\circ$ ), both accelerated and decelerated three-dimensional boundary layers show significantly greater capacity for algebraic growth than two-dimensional boundary layers at equivalent Reynolds numbers, subjected to identical pressure gradients. More algebraic growth occurs in retarded boundary layers, a finding consistent with results for the two-dimensional case. The sweep angle which maximizes growth does not correspond to that which induces the largest crossflow component in the base flow.

In the adverse pressure gradient boundary layer considered here algebraic, crossflow and Tollmien–Schlichting growth mechanisms are simultaneously active in different areas of the wavenumber plane. In contrast to the two-dimensional case, the region of the wavenumber plane where optimal perturbations experience the most growth coincides with a region of exponential instability. This confirms that these two essentially inviscid mechanisms amplify structurally similar disturbances.

This coincidence is explored further for the supercritical flow of the DLR experiments. It is shown that while the strong growth of the modal mechanism dwarfs algebraic growth over long periods, transient growth is appreciable for sufficiently short intervals. Working from this observation, two paths by which optimal perturbations may affect crossflow transition are outlined. It is plausible that the algebraic growth mechanism investigated here constitutes a preferential receptivity path for selecting steady crossflow modes.

Despite the limitations of the temporal approach employed in this study, transient growth phenomena are clearly of some consequence in three-dimensional boundary layers. Recent analyses confirming the importance of taking curvature and non-parallel effects into account when studying crossflow instability on swept wings indicate that an extension of the current work to the spatial framework is not readily apparent (Högberg & Henningson 1998; Haynes & Reed 2000).

P. C. was supported by Swiss National Science Foundation grant 2100-52'592.97. It is a pleasure to thank Professors L. Kleiser and P. Luchini for questions, suggestions and enjoyable discussions which improved the manuscript.

#### REFERENCES

- ABERGEL, F. & TÉMAM, R. 1990 On some control problems in fluid mechanics. *Theor. Comput. Fluid Dyn.* **1**, 303–325.

- ANDERSSON, P., BERGGREN, M. & HENNINGSON, D. S. 1999 Optimal disturbances and bypass transition in boundary layers. *Phys. Fluids* **11**, 134–150.
- BIPPE, H. 1999 Basic experiments on transition in three-dimensional boundary layers dominated by crossflow instability. *Prog. Aero. Sci.* **35**, 363–412.
- BREUER, K. S. & KURAI, T. 1994 Transient growth in two- and three-dimensional boundary layers. *Phys. Fluids* **6**, 1983–1993.
- BUTLER, K. M. & FARRELL, B. F. 1992 Three-dimensional optimal perturbations in viscous shear flow. *Phys. Fluids* **4**, 1637–1650.
- CANUTO, C., HUSSAINI, M. Y., QUARTERONI, A. & ZHANG, T. 1988 *Spectral Methods in Fluid Dynamics*. Springer.
- COOKE, J. C. 1950 The boundary layer of a class of infinite yawed cylinders. *Proc. Camb. Phil. Soc.* **46**, 645–648.
- CORBETT, P. & BOTTARO, A. 2000 Optimal perturbations for boundary layers subject to stream-wise pressure gradient. *Phys. Fluids* **12**, 120–130.
- COSSU, C., CHOMAZ, J.-M., HUERRE, P. & COSTA, M. 2001 Maximum spatial growth of Görtler vortices. To appear in *Flow, Turb. & Combust.*
- DRAZIN, P. G. & REID, W. H. 1981 *Hydrodynamic Stability*. Cambridge University Press.
- ELLINGSEN, T. & PALM, E. 1975 Stability of linear flow. *Phys. Fluids* **18**, 487–488.
- FARRELL, B. F. 1988 Optimal excitation of perturbations in viscous shear flow. *Phys. Fluids* **31**, 2093–2102.
- GRAY, W. E. 1952 The effect of wing sweep on laminar flow. *Tech. Rep.* RAE TM Aero 255. British Royal Aircraft Establishment.
- GREGORY, N., STUART, J. T. & WALKER, W. S. 1955 On the stability of three-dimensional boundary layers with application to the flow due to a rotating disk. *Proc. R. Soc. Lond. A* **248**, 155–199.
- GUNZBURGER, M. D. 2001 Adjoint equation-based methods for control problems in incompressible, viscous flows. To appear in *Flow, Turb. & Combust.*
- HANIFI, A. & HENNINGSON, D. S. 1998 The compressible inviscid algebraic instability for streamwise independent disturbances. *Phys. Fluids* **10**, 1784–1786.
- HAYNES, T. S. & REED, H. L. 2000 Simulation of swept-wing vortices using nonlinear parabolized stability equations. *J. Fluid Mech.* **405**, 325–349.
- HILL, D. C. 1995 Adjoint systems and their role in the receptivity problem for boundary layers. *J. Fluid Mech.* **292**, 183–204.
- HÖGBERG, M. & HENNINGSON, D. 1998 Secondary instability of cross-flow vortices in Falkner-Skan-Cooke boundary layers. *J. Fluid Mech.* **368**, 339–357.
- HULTGREN, L. S. & GUSTAVSSON, L. H. 1981 Algebraic growth of disturbances in a laminar boundary layer. *Phys. Fluids* **24**, 1000–1004.
- LANDAHL, M. T. 1980 A note on an algebraic instability of inviscid parallel shear flows. *J. Fluid Mech.* **98**, 243–251.
- LASSEIGNE, D. G., JOSLIN, R. D., JACKSON, T. L. & CRIMINALE, W. O. 1999 The transient period for boundary layer disturbances. *J. Fluid Mech.* **381**, 89–119.
- LUCHINI, P. 1996 Reynolds-number-independent instability of the boundary layer over a flat surface. *J. Fluid Mech.* **327**, 101–115.
- LUCHINI, P. 2000 Reynolds-number-independent instability of the boundary layer over a flat surface: optimal perturbations. *J. Fluid Mech.* **404**, 289–309.
- LUCHINI, P. & BOTTARO, A. 1998 Görtler vortices: a backward-in-time approach to the receptivity problem. *J. Fluid Mech.* **363**, 1–23.
- MEYER, F. 1989 Numerische Simulation der Transition in dreidimensionalen Grenzschichten. PhD thesis, Universität Karlsruhe, Fakultät für Maschinenbau; also *DLR Rep.* DLR-FB 89-12.
- MEYER, F. & KLEISER, L. 1990 Numerical simulation of transition due to crossflow instability. In *Laminar-Turbulent Transition: IUTAM Symposium Toulouse/France 1989* (ed. D. Arnal & R. Michel), pp. 609–619. Springer.
- PRESS, W. H., TEUKOLSKY, S. A., VETTERLING, W. T. & FLANNERY, B. P. 1992 *Numerical Recipes in C*, 2nd edn. Cambridge University Press.
- RADEZTSKY, R. H., REIBERT, M. S. & SARIC, W. S. 1999 Effect of isolated micron-sized roughness on transition in swept-wing flows. *AIAA J.* **37**, 1370–1377.
- REDDY, S. C. & HENNINGSON, D. S. 1993 Energy growth in viscous channel flows. *J. Fluid Mech.* **252**, 209–238.

- REED, H. L. & SARIC, W. S. 1989 Stability of three-dimensional boundary layers. *Ann. Rev. Fluid Mech.* **21**, 235–284.
- REED, H. L., SARIC, W. S. & ARNAL, D. 1996 Linear stability theory applied to boundary layers. *Ann. Rev. Fluid Mech.* **28**, 389–428.
- TREFETHEN, L. N., TREFETHEN, A. E., REDDY, S. C. & DRISCOLL, T. A. 1993 Hydrodynamic stability without eigenvalues. *Science* **261**, 578–584.
- WEIDEMAN, J. A. C. & REDDY, S. C. 2000 A MATLAB differentiation matrix suite. *ACM Trans. Math. Soft.* **26** (4). Available at <http://ucs.orst.edu/~weidemaj/differ.html>